Received: 2 August 2023 | Revised: 31 January 2024 | Accepted: 2 February 2024

DOI: 10.1002/jbm.a.37686

RESEARCH ARTICLE

Society For Biomaterials | WILEY

Lithium-loaded GelMA-Phosphate glass fibre constructs: Implications for astrocyte response

Zalike Keskin-Erdogan[1,2] | Nandin Mandakhbayar[3] | Gang Shi Jin[3] | Yu-Meng Li[3] | David Y. S. Chau[1,4] | Richard M. Day[5] | Hae-Won Kim[2,4,6] | Jonathan C. Knowles[1,4]

[1]Division of Biomaterials and Tissue Engineering, Eastman Dental Institute, University College London, Royal Free Hospital, London, UK

[2]Chemical Engineering Department, Imperial College London, London, UK

[3]Institute of Tissue Regeneration Engineering (ITREN), Dankook University, Cheonan, Republic of Korea

[4]UCL Eastman-Korea Dental Medicine Innovation Centre, Dankook University, Cheonan, Republic of Korea

[5]Centre for Precision Healthcare, UCL Division of Medicine, University College London, London, UK

[6]Department of Nanobiomedical Science and BK21 NBM Global Research Center for Regenerative Medicine, Dankook University, Cheonan, Republic of Korea

Correspondence
Zalike Keskin-Erdogan and Jonathan C. Knowles, Division of Biomaterials and Tissue Engineering, Eastman Dental Institute, University College London, Royal Free Hospital, London, UK.
Email: zalike.keskin.17@ucl.ac.uk and j.knowles@ucl.ac.uk

Funding information
Republic of Turkiye Ministry of National Education; National Research Foundation of Korea, Grant/Award Numbers: MRC2021R1A5A2022318, RS-2023-00220408

Abstract

Combinations of different biomaterials with their own advantages as well as functionalization with other components have long been implemented in tissue engineering to improve the performance of the overall material. Biomaterials, particularly hydrogel platforms, have shown great potential for delivering compounds such as drugs, growth factors, and neurotrophic factors, as well as cells, in neural tissue engineering applications. In central the nervous system, astrocyte reactivity and glial scar formation are significant and complex challenges to tackle for neural and functional recovery. GelMA hydrogel-based tissue constructs have been developed in this study and combined with two different formulations of phosphate glass fibers (PGFs) (with Fe^{3+} or Ti^{2+} oxide) to impose physical and mechanical cues for modulating astrocyte cell behavior. This study was also aimed at investigating the effects of lithium-loaded GelMA-PGFs hydrogels in alleviating astrocyte reactivity and glial scar formation offering novel perspectives for neural tissue engineering applications. The rationale behind introducing lithium is driven by its long-proven therapeutic benefits in mental disorders, and neuroprotective and pronounced anti-inflammatory properties. The optimal concentrations of lithium and LPS were determined *in vitro* on primary rat astrocytes. Furthermore, qPCR was conducted for gene expression analysis of GFAP and IL-6 markers on primary astrocytes cultured 3D into GelMA and GelMA-PGFs hydrogels with and without lithium and *in vitro* stimulated with LPS for astrocyte reactivity. The results suggest that the combination of bioactive phosphate-based glass fibers and lithium loading into GelMA structures may impact GFAP expression and early IL-6 expression. Furthermore, GelMA-PGFs (Fe) constructs have shown improved performance in modulating glial scarring over GFAP regulation.

KEYWORDS
bioactive glass, biomaterial, GFAP, glial scar, hydrogel, IL-6, neural recovery

1 | INTRODUCTION

Biomaterials have been extensively investigated for delivering compounds such as active drugs, neurotrophic factors, and growth factors in neural tissue engineering applications.[1–4] In particular, hydrogel systems enable the easy incorporation of drugs and bio-compounds, and delivery can be designed to be self-assembled or controlled.[5,6] In the central nervous system (CNS), astrocytes play a crucial role in the survival and growth, synapse formation, and maturation of neurons.[7] Spinal cord injuries (SCIs) often cause astrogliosis (astrocyte reactivity/glial scars), characterized by cytokine secretion leading to inflammation, neurodegeneration, and apoptosis.[7–9] Reactive astrocytes produce increased intermediate filaments like glial fibrillary acidic proteins (GFAPs) and chondroitin sulfate proteoglycans (CSPGs).[10,11] GFAP is exclusively present in astrocytes and serves as a marker for the correct phenotype[12] while, IL-6 is responding to infections and injuries, modulating pathways could impact repair, inflammation.[13] Glial scars, formed post-injury, have dual effects: positive ones such as reconstructing the blood–brain barrier and protection against external inflammation.[10] However it also can create an inhibitory microenvironment for neural recovery like promoting inflammation, and apoptosis is associated with glial scars and continuing astrocyte reactivity.[14,15] Despite the absence of validated therapies for severe neural injuries, promising research suggests potential avenues for modulating glial scar and astrocyte reactivity to enhance neural recovery.[15–18]

In this study lithium administrated via an engineered biomaterial construct of GelMa-PGFs to assess its performance in response to stimulated increased GFAP expression with primary astrocytes was carried out. Lithium has been utilized as a treatment for various mental disorders such as depression, bipolar disorder, and schizophrenia. Studies also suggest that it may have a role in protecting neurons from damage. Research has shown that therapeutic doses of lithium have a positive effect, and it also has significant anti-inflammatory properties by reducing the expression of pro-inflammatory cytokines and chemokines.[19–21] Lithium doping of bioactive glasses has been previously shown to improve early-stage osseointegration and bone remodeling *in vivo*.[22] In parallel, Jin et al.[23] have also reported that lithium chloride enhances bone regeneration, and osseointegration with implants in osteoporotic conditions *in vivo* on rats. Given the encouraging results observed and the utilization of lithium in clinical settings, the motivation behind incorporating lithium as a bioactive material in this study is to explore its potential beneficial effects. The objective is to investigate its incorporation into GelMA-PGFs, with the aim of facilitating neural tissue engineering applications. Our previous study on phosphate glass fibers (PGFs) and GelMA has thoroughly characterized these two biomaterials for tissue engineering purposes.[24] The rationale for selecting GelMA as the foundational biomaterial for this construct lies in its tuneable mechanical properties as well as biocompatibility with many types of cells. In this continuing study, the aim was to determine GFAP and IL-6 expression in response to lithium administration to LPS-stimulated reactive astrocytes cultured 3D into GelMA, GelMA-PGFs(Ti) and GelMA-PGFs (Fe) hydrogels, as well as exploring *in vivo* biocompatibility of GelMA-PGFs. The result of this work suggested that the combination of bioactive phosphate-based glass fibers and lithium loading into GelMA structures may help modulate GFAP expression and early IL-6 expression on primary astrocytes that have been cultured in 3D GelMA and GelMA-PGFs hydrogels which have been exposed to LPS to initiate their reactivity.

2 | EXPERIMENTAL

2.1 | Development of PGFs incorporated GelMA Hydrogel (GelMA-PGFs)

GelMA was synthesized, in-house, as described in our previous work.[24] A GelMA solution was prepared using 10 wt % in PBS and supplemented with 0.1% (w/v) lithium phenyl-2,4,6-trimethylbenzoylphosphinate (LAP) photo-initiator and subsequently the pH of the polymer solution was adjusted to 7.3 by using 1 M of HCl and/or NaOH. For the preparation of PGFs, the method was used as previously described in the study by Ahmed et al. (2004)[24,25] with two different formulations of phosphate-based glasses as *50 P_2O_5–40 CaO–5 Na_2O–5 Fe_2O and 50 P_2O_5–35 CaO–10 Na_2O–5 TiO_2 (*number prefix of the oxides represent mol percentages) were designated as PGFs(Fe) and PGFs(Ti), respectively. As previously described; the casting of PGFs structured hydrogels was performed by placing a sterile fiber bundle into the bottom of a low adherence 96-well cell culture plate (CellStar, Greiner Bio-One, UK) and parallel aligned by using fine-tip tweezers. Thereafter, 100 μL of 10 wt % GelMA (including 0.1%[w/v] LAP) solution was pipetted on top of PGFs (PGFs–GelMA ratio kept at 2% w/v [mg/μL]).[24] Following trypsinization pertinent cells (C6 or primary astrocytes—R-HiAst-521) suspended in culture media (10^6 cells/mL), 10 μL of cell solution was subsequently mixed into the gels resulting in a final cell concentration of 1000 cells per sample. The plate then was gently shaken in a flat platform laboratory shaker for 5 min. Lastly, the plate was taken to a UV chamber (XYZ Printing Model 3UD10, Taiwan, UV LED λ 375–405 nm, 16 W) and photo crosslinked for 60 s. Then the appropriate cell culture medium was supplemented, and *in vitro* 3D cell culture was started at 37°C, 5% CO_2, and humidified conditions.

The Molecular Probes® Neurite Outgrowth Staining Kit (A15001, Invitrogen™, ThermoFisher Scientific, UK) kit was utilized to visualize neurite outgrowth on unfixed live C6 cells that were 3D cultured into GelMA and GelMA-PGFs hydrogels. Based on the supplier's instructions, the staining protocol was applied to unfixed live cells into hydrogels and was imaged on a fluorescence microscope (Leica, DM IRB, UK).

2.2 | *In vivo* biocompatibility of GelMA and GelMA-PGFs Constructs

The *in vivo* biocompatibility was investigated by implanting the scaffolds subcutaneously under the skin tissue of Sprague–Dawley,

healthy, male 5-week-old rats, the number of constructs implanted per rat per time point was 4, and at 2 and 4 weeks of post-operation samples, were harvested for immunohistology examination. The animals were cared for in separated cages under a controlled environment with food and water provided ad libitum following guidelines approved by the Animal Care and Use Committee at Dankook University, Republic of Korea (DKU-21-031). Four replicates for each experimental group of GelMA, GelMA-PGFS(Fe), and GelMA-PGFs(Ti) were used for this study. The surgery was performed under general anesthesia using air inspiration with Isoflurane (Ifran solution, South Korea). The dorsal area of skin hair was trimmed and disinfected with iodine and 70% ethanol solution. The samples were then implanted in the subcutaneous pocket separately. The skin was sutured with non-absorbable suture material (4–0 Prolene, Ethicon, Germany). At predetermined time points of 2 and 4 weeks, animals were euthanased by CO_2 inhalation. The implants and surrounding tissue with scaffolds were harvested and fixed in 10% neutral buffered formalin for 24 h at room temperature (~19°C) and then wax embedded. Histological sections were cut by a semi-automated rotary microtome (Leica RM2245, Leica Biosystems, Germany), and 5 µm coronal sections of the central area at the samples were prepared to coated glass slides. The slides with tissue sections were deparaffinized and hydrated through a series of xylene and graded ethanol solutions. Stained with hematoxylin and eosin (H&E) was performed and images were captured under a light microscope (IX71, Olympus, Japan).

For immunohistochemical staining (IHC), the tissue sections were rehydrated and then heated with an antigen-retrieval solution of 0.01 M citrate buffer (pH 6) for 15 min at 95°C, followed by treating DAKO blocking solution (Agilent, Dako) for 30 min, then incubated with primary antibodies (CD3, Rabbit, ab16669, Monoclonal, Abcam; and F4/80, Rat monoclonal, ab16911, Abcam) at 4°C overnight for staining. For the secondary antibody binding, the slides were incubated with secondary antibodies, including Rhodamine (TRITC)-conjugated donkey Anti-Rabbit (Jackson, Lab. Inc., USA) and FITC-conjugated goat Anti-Rat (NOVUS), for 1 h at room temperature (~19°C), finally DAPI (Invitrogen) was used for counterstaining. The images were taken under a confocal laser scanning microscope (CLSM; Zeiss LSM 700, Germany) and analyzed with Image J.

2.3 | Growing primary astrocytes

Primary rat astrocytes named R-HiAst-521 were purchased from Lonza (Catalog #: R-HiAs-521, Lonza, USA). To grow the primary astrocytes the recommended media (Astrocyte Growth Medium Bulletkit® which contains 500 mL ABM™ (Astrocyte Basal Medium) (CC-3187)) and AGM™ Singlequots® Supplement pack (CC-4123) containing 15.0 mL FBS, 5.00 mL L-glutamine, 0.50 mL gentamicin, 0.50 mL ascorbic acid, 0.50 mL HEGF, and 1.25 mL insulin by the provider was used. Then cells were incubated for 4 h initially at 37°C, 5% CO_2 incubator to condition cells followed by changing media to fresh pre-warmed medium. Every 4–5 days, 50% of the media was changed with a fresh growth medium, and when cells were confluent, they were subcultured and replated at a subculture ratio of 1:3.

2.4 | Determination of optimal concentration of lithium and LPS *in vitro*—metabolic activity and LDH assays

Prior to treating cells with lithium chloride and LPS, to determine the safe concentration of lithium and the effect of LPS on cells, a range of different concentrations of each were applied to R-HiAs-521 cells cultured on 3D GelMA hydrogels. Both LPS and lithium were applied via addition to culture medium with no serum supplementation. Different lithium concentrations in the culture were adjusted by using 1 M $LiCl_2$ stock solution that was premade in PBS (without Ca, Mg). Likewise, to determine the noncytotoxic dose of LPS used *in vitro*, final concentrations from 50 to 5000 ng/mL in the culture medium were tested. To assess cell viability and cytotoxicity levels, metabolic activity analyses with AlamarBlue and LDH assays (The CytoTox 96® Non-Radioactive Cytotoxicity Assay, PromegaG1780) were used. These assays were used according to the manufacturer's directions and the readout of absorbance was recorded at 490 nm within an hour after adding the stop solution using the Tecan Infinite M200 Plate reader. All test and control groups were performed in triplicate.

2.5 | Lithium loading into GelMA hydrogels

$LiCl_2$ (1 M) working stock solution of $LiCl_2$ in PBS was filter sterilized by using a 0.22 µm sterile syringe filter. Then, the calculated volume to make the final lithium concentration of 1 mM $LiCl_2$ in the gel solution was added and mixed into the desired amount of GelMA solution (10 wt %) that was subsequently mixed with 0.1% w/v LAP. Since lithium chloride makes the pH of the solution acidic, it was adjusted back to pH 7.4. Finally, this solution (called GelMA/Li) was cast into 96-well plates with 100 µL of volume and photo-crosslinked for 60s under UV (XYZ Printing Model 3UD10, Taiwan, UV LED λ 375–405 nm, 16 W). Determining the release profile of lithium loaded into the GelMA hydrogel structure, GelMA samples were soaked in deionized water (DI) (GelMA/DI ratio was kept at 1:50 v/v) for 14 days and for the time points of 1, 3, 5, 6, 7, and 14 days, the water was collected for testing and replaced with fresh DI. For released lithium-ion detection, ICP-OES (Agilent Technologies-Varian 720-ES, Santa Clara, CA 95051, USA) was used and cumulative lithium release was plotted with OriginPro.

2.6 | Immunofluorescence analysis

Briefly, primary R-hiAs-521 cells were cultured for 3D, in GelMA and GelMA-PGFs hydrogels in the presence and absence of Li. Seventy-two hours after cells were left to recover from LPS treatment, prior to

fixation samples were washed three times with ice-cold PBS and fixed with 4% paraformaldehyde in PBS (pH 7.4) for 10 min at room temperature (~19°C). Since the target protein of GFAP is intracellular, cell permeabilization was done by incubating samples in 0.1% Triton X-100 containing PBS for 10 min, then samples were washed with fresh PBS three times for 5 min. Then, for blocking the unspecific binding of the antibody, samples were incubated with 1% BSA, 22.52 mg/mL glycine in PBST (PBS containing 0.1% Tween 20) for 30 min. Then for primary antibody staining GFAP Astro (0.2 mg/mL) (Mouse, IgG, Monoclonal antibody) diluted in 1% BSA in PBST in the ratio of 1:100 to 1 µL/mL and applied to samples at a volume of ~250 µL, making sure to submerge the entire gels and incubated for 1 h at room temperature (~19°C) or overnight at 4°C. Afterward, the solution was decanted, and samples were washed three times in PBS, for a minimum of 5 min.

Following the wash, a secondary antibody Goat Anti-Mouse IgG-H&L AlexaFlour (Green color, 2 µg/mL) in 1% BSA was applied to samples and incubated for 1 h at room temperature (~19°C) in the dark. Then, the solution was decanted, and samples were washed three times with PBS for 5 min each in the dark. Finally, gels were incubated for counterstaining in 300 nM DAPI (blue color, DNA stain) and for 1–3 min, and Propidium Iodide (red color, 1 mg/mL) was added and then rinsed with PBS. For confocal microscopy imaging (Aurox, UK) with Visionary Software (Aurox, UK) was used and to provide prolonged and strong fluorescence, ProLong™ Gold Antifade Mountant was applied to the gel sample prior to imaging. All images were processed via ImageJ/FiJi software for color merging, scale bar setting, and brightness adjustments.

2.7 | qPCR analysis

R-hiAs-521 primary astrocytes at passage 4 were seeded at a concentration of 10^5 cells/scaffold into GelMA only as a control, and GelMA-PGFs (Ti), GelMA-PGFs (Fe) with and without lithium loading (sample coding details for this experiment were as presented in Table 1). Following 36 h of initiation of 3D cell culturing apart from one GelMA-only control group, each group was treated with 1 µg/mL LPS for 24 h to stimulate *in vitro* LPS-mediated astrocyte reactivity and elevation of inflammatory response. qPCR was run to verify the upregulation of GFAP and IL-6 gene expression in 24 h with just GelMA and GelMA/Li constructs. All groups were then further left to recover in culture with replaced fresh media for a further 72 h to evaluate the effect of the presence of PGFs and Li on the downregulation of GFAP expression. For the qPCR assay, a Cells to Ct kit (Ambion, AM1728) was used per the manufacturer's protocol. This kit does not require steps for RNA isolation for cDNA acquisition as it provides the appropriate reagents for direct cDNA extraction from cells. As cells were 3D cultured in a hydrogel to release the cells from the hydrogel network, prior to using this kit, standard trypsinization was applied with the modifications of extended time and use of collagenase and mechanical disruption of the scaffold. Briefly, following media removal, samples were robustly washed with PBS (without Ca, Mg) five times, until the pink media color staining in the gels had faded significantly. Then the gel samples were cut into small pieces with the tip of a sterile spatula to increase the surface area for the enzyme mix. Then, 0.25% Trypsin/EDTA solution mixed with 0.5 mg/mL collagenase (>125 CDU, from Clostridium histolyticum, Sigma) was applied 200–250 µL to each group and incubated over 15 min in a 37°C incubator. The population of detached cells was observed under an inverted light microscope (Olympus CK2, UK) the complete degradation of gels was not completed since this would take longer which then may cause other changes in the cells. Cells were counted using a hemacytometer and 1000 cells from each sample and to remove genomic DNA during cell lysis, prior to starting the lysis, DNase I was diluted in the lysis solution (1:100) and 50 µL of lysis solution was used. All samples were taken to further steps for RT-PCR, and a thermal cycler (PTC-100219 Programmable Thermal Controller MJ Research, Inc., Canada) was used to obtain cDNA.

cDNA was prepared for qPCR with Gene expression assays targeting each candidate gene for GFAP and IL-6 and were purchased from ThermoFisher Scientific TaqMan. A real-time PCR instrument (Applied Biosystems 7300 Real-Time PCR System) was programmed to (2 min at 50°C, 10 min at 95°C, and 40 PCR cycles for 15 s at 95°C). The primer markers used were all from TaqMan® Gene Expression Assays (ThermoFisher, Scientific, UK) for this experiment were GFAP (Build 6.0 Rat Chr.10: Rn00566603_m1, Rattus norvegicus glial fibrillary acidic protein (GFAP), mRNA, NCBI Reference Sequence: NM_017009.2), and IL-6 (Build 6.0 Rat Chr.4: 221 Rn01410330_m1, *Rattus norvegicus* interleukin 6 (IL-6), mRNA, NCBI Reference Sequence: NM_012589.2). The housekeeping gene was GAPDH (Build 6.0 Rat Chr.4: Rn01775763_g1, *R. norvegicus* glyceraldehyde-3-phosphate dehydrogenase (GAPDH), mRNA, NCBI Reference Sequence: NM_017008.4). The analysis involved viewing the amplification plots for the entire plate, setting the baseline and threshold values, and using comparative cycle threshold (Ct) values. In order to compare multiple samples, one of the samples, which was GelMA only with no LPS treatment, was chosen as the calibrator, and the expression of the target genes (GFAP and IL-6) in all other samples is expressed as an increase (up-regulated) or decrease (down-regulated) relative to the calibrator. To determine relative quantification, all Ct values of targeted genes of the samples were normalized to a reference gene (GAPDH in this work). For determining the expression level

TABLE 1 Samples details have been used in qPCR and IF analyses.

Sample code	LPS	Lithium
1. GelMA (only) control	–	–
2. GelMA (only)	+	–
3. GelMA-PGFS(Ti)	+	–
4. GelMA-PGFs(Fe)	+	–
5. GelMA/Li	+	+
6. GelMA/Li-PGFs(Ti)	+	+
7. GelMA/Li-PGFs(Fe)	+	+

of the gene of interest in the test sample relative to the calibrator sample, as a widely chosen method, Livak's method ($2^{-\Delta\Delta Ct}$) was used.

2.8 | Statistical analyses

The data are "mean" ± SD and all the graphs were produced on OriginPro 2021. For statistics, normality was checked first by using the Kolmogorov–Smirnov test, and when only the data cannot reject normality parametric ANOVA with post hoc tests of Tukey's and Bonferroni's, were used. All the error bars represent ± standard deviation. The *p* values were taken as an indicator of significant difference as follows *($p < .05$) and **($p < .01$) ***($p < .001$).

3 | RESULTS

Enzymatic accelerated degradation tests for biomaterials are often carried out *in vitro* to evaluate the stability and enzymatic degradability performance of biomaterials by using MMP enzymes. An accelerated degradation run with collagenase showed that the half-life of GelMA only was 1.8 h, and for GelMA-PGFs hydrogels it was 1.2 h (Figure S1). Optical images were added to the accelerated degradation plot from gels to show the physical appearance of gels over the course of the degradation experiment. After 2.5 h, all gels were degraded, and for GelMA-PGFs samples, only PGF bundles remained. As biomaterials, both GelMA and PGFs have been proven to be biodegradable *in vivo*.[26–28] It was determined that due to the presence of PGF bundles in GelMA that interrupt the physical integrity of the hydrogel and increase the surface area of the substrate for the enzyme, a decreased half-life for GelMA-PGFs (Fe and Ti) has been recorded.

To explore the *in vitro* biocompatibility of the PGF constructs, the astrocytes were cultured in the scaffolds for up to 14 days through viability and cell membrane integrity, a fluorescence staining kit (Neurite Outgrowth Staining Kit, Invitrogen, A15001) has been used. In Figure 1, fluorescence images were taken from GelMA, GelMA-PGFs(Fe), and GelMA-PGFs(Ti) hydrogels at day 14, cells were cultured in 3D; hence they are in different layers within the hydrogel network. Cell viability indicated by the green color and membrane integrity and extension with red color have been observed. The red color represents membrane integrity and stains the whole membrane of neural cells while green and blue are live cell indicators. Cells that were cultured in GelMA-PGFs(Ti) have shown a relatively stronger intensity of cell membrane stain of neurite outgrowth red fluorescence (Figure 2).

Histological examination of H&E stained samples after 2 and 4 weeks of implantation showed that all the implanted samples gave rise to some inflammatory cells and infiltrated blood cells. At 2 weeks, the thickness of the fibrous capsule was observed to be in the order GelMA < GelMA-PGFs(Fe) < GelMA-PGFs(Ti), but it became less thick and denser around the gel scaffolds overtime at 4 weeks. Immunohistochemistry staining using F4/80 and CD3 markers showed that

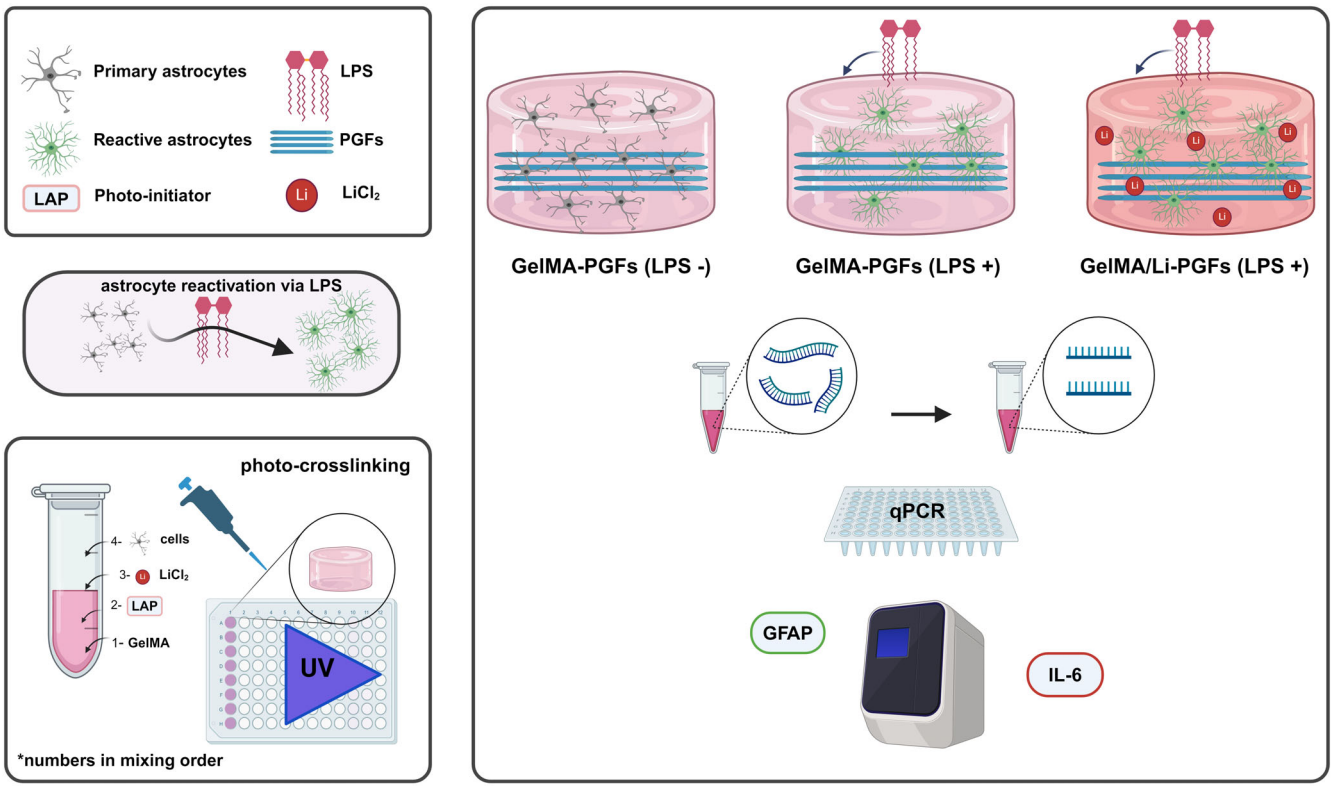

FIGURE 1 Visual summary of the experimental procedures in the study.

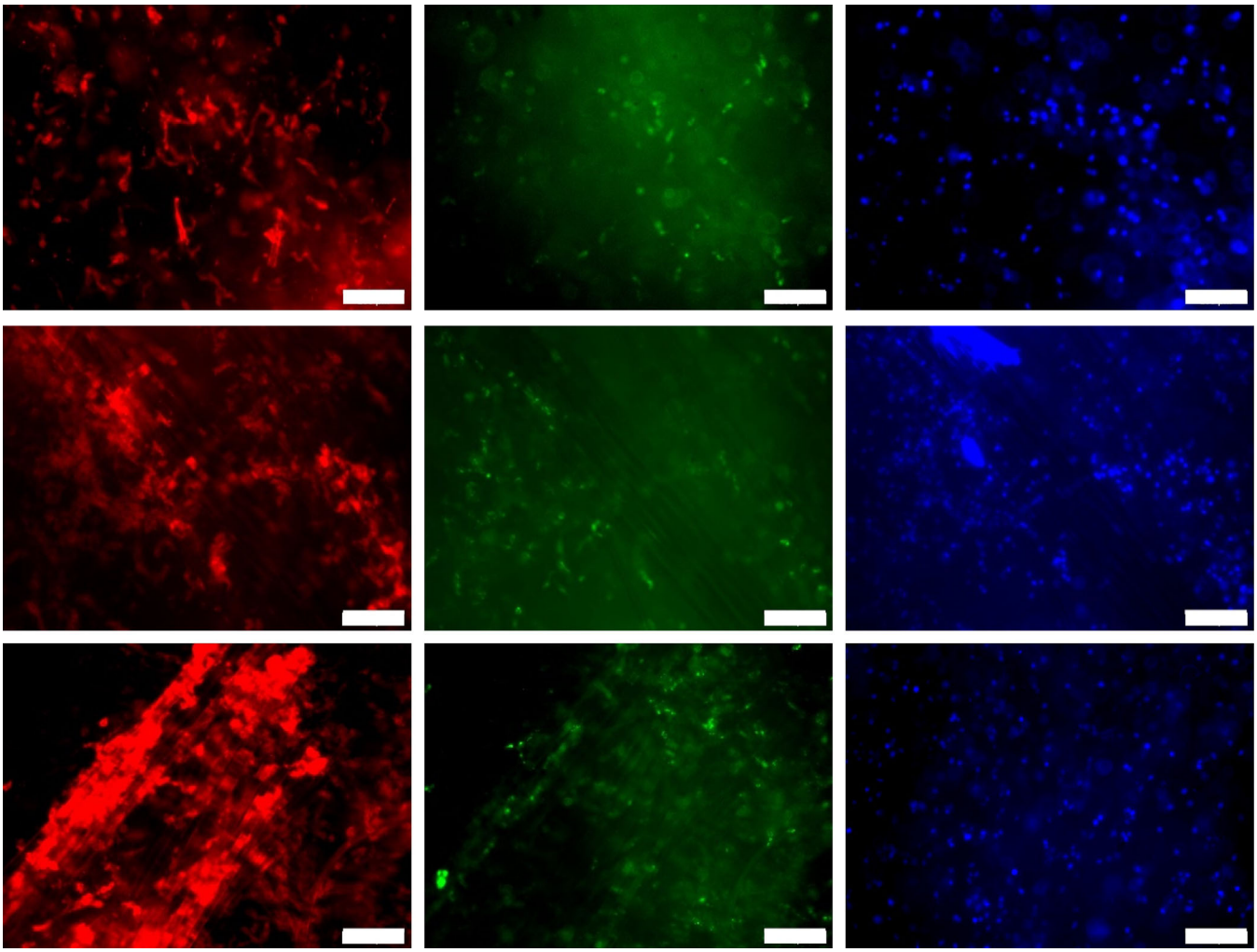

FIGURE 2 Fluorescent images taken at D14 belong to GelMA, GelMA-PGFs(Fe), and GelMA-PGFs(Ti) hydrogels, respectively, in row order. The red stain is for cell membrane, and the green indicates cell viability since the green color was not stable. Supplementary Hoechst counterstaining applied as the live-cell indicator. Scale bars 200 nm.

GelMA and GelMA-PGFs(Fe) groups expressed higher levels of F4/80 and CD3, but the fibrous capsule was thinner than that of GelMA-PGFs(Ti). On the other hand, the GelMA-PGFs(Ti) group showed lower levels of F4/80 and CD3 expression, but the fibrous capsule was thicker. After 4 weeks, the expression of F4/80 and CD3 decreased in the GelMA and GelMA-PGFs(Fe) groups, but it increased in the GelMA-PGFs(Ti) group. Overall, GelMA appeared to be more compatible than the other groups, showing a thinner layer of fibrous tissue and a decrease in macrophage and foreign body reaction over time.

Different concentrations of lithium, ranging from 1 mM to 10 mM, were tested to observe their impact on 3D cultured astrocytes within GelMA hydrogels. The metabolic activity and cytotoxicity results were recorded for up to 7 days using the Alamar Blue metabolic activity and LDH methods, respectively. The findings have shown that the introduction of lithium via GelMA hydrogels was less harmful than direct application via culture media. This was inferred from the insignificant difference in metabolic activity results of all lithium concentrations with the control, even at 10 mM (Figure 3). In contrast, the levels of LDH release were found to be associated with higher concentrations of lithium, as shown in Figure 4. $LiCl_2$ tends to lower the pH to below neutral levels, but when combined with GelMA solution, the pH was adjusted to 7.4.

Experiments with varying concentrations of LPS between 5 μg/mL and 50 ng/mL (5000, 1000, 500, 100, and 50 ng/mL) to investigate their effects on the metabolic activity and cell death of primary astrocytes have shown that on the first and third day of the experiments, a moderate increase in metabolic activity with increasing LPS concentrations compared to the control group (no LPS applied astrocytes cultured into GelMA) was seen as shown in Figure 4. This may be associated with the triggered activity of astrocytes since there was no significant increase in LDH release (Figure 3), thus, there was no significant cell death initiated with LPS treatment. Based on the 3D network structure of hydrogels and their ability to act as a barrier membrane to slow down release[29] may create a supportive encapsulating environment for 3D cultured cells, it is believed that a higher

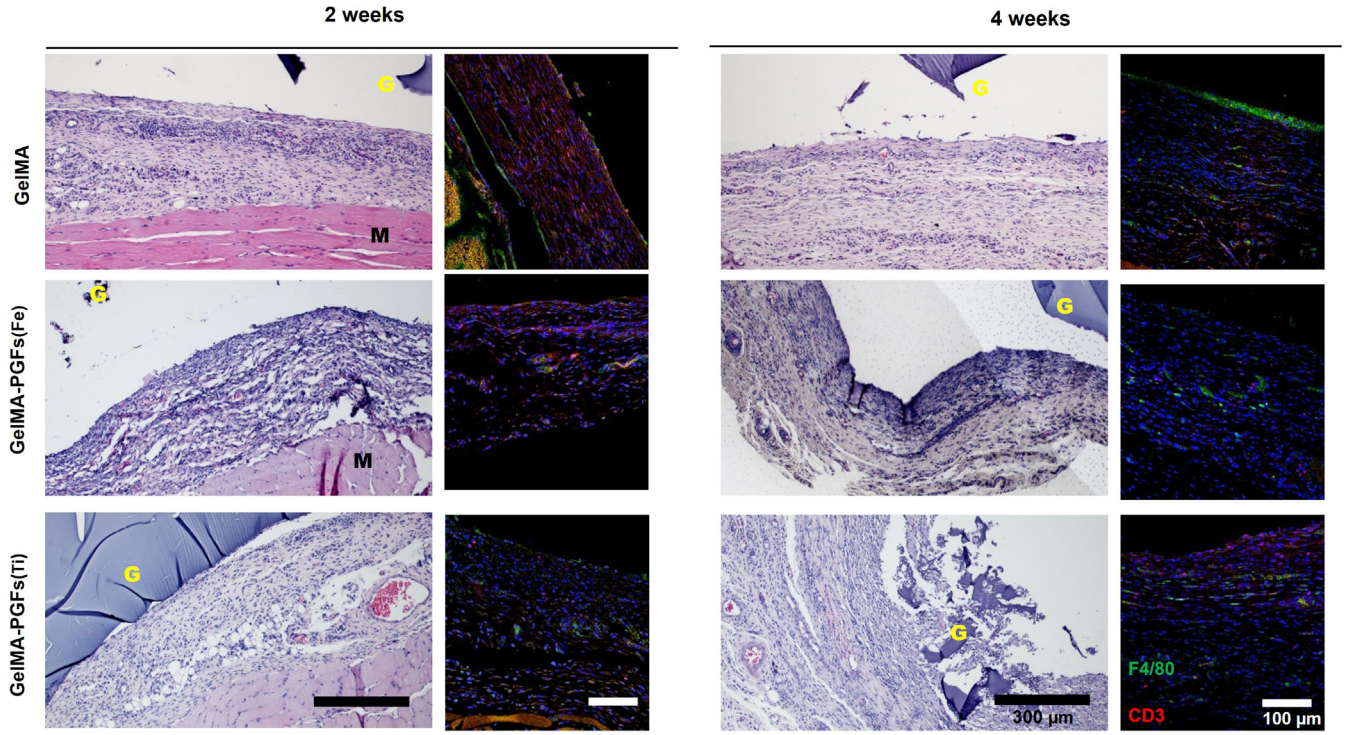

FIGURE 3 H&E and IF images of tissue sections for GelMA and GelMA-PGFs samples harvested 2 and 4 weeks after transplantation (Scale bars 100 µm and applies IF images and 300 µm for all H&E images seen) ("G" is for where GelMA and GelMA-PGFs samples implanted and "M" is for muscle tissue) F4/80-Green (macrophage marker) and CD3-Red (T-cell co-receptor) DAPI- Blue (Counter-stain for nuclear double-strained DNA).

concentration of LPS may be required to trigger astrocyte reactivity *in vitro*.

Maximum cell death was observed via LDH results after 48 h, with 10 mM of lithium loaded into GelMA which has been found to be significantly lower than the negative control which represents LDH number of lysed cells ($p < .001$) but was not significantly different from control group which did not have lithium added ($p < .05$). The lowest LDH amount was obtained with the 1 mM of lithium loaded group and this group has shown improved metabolic activity results on cells *in vitro* (Figure 4) in early culture periods (D1 and D2) so that for the future experiment this lithium concentration of 1 mM was chosen and which has also been found to parallel related works in the field.[20,30,31]

The release of lithium from GelMA hydrogels was analyzed by immersing them in ultrapure water for 2 weeks, after being loaded with a 1 mM solution of $LiCl_2$. The cumulative release of lithium was monitored by using fresh UPW at every time point, and the results were plotted and shown in Figure 4. It was observed within the first 3 days lithium was released, with a maximum concentration of 0.80 ppm. Subsequently, there was only a small amount of lithium released over the next 2 weeks, indicating that the GelMA hydrogels could maintain lithium within its structure in cells cultured 3D within the gels.

The effects of lithium and PGFs(Fe) on GFAP and IL-6 expression in astrocytes were investigated. The results showed that the presence of lithium increased GFAP expression more than LPS alone in the first 24 h. However, IL-6 expression was moderately downregulated in the presence of lithium, but this was not statistically significant ($p > .05$). The potential anti-inflammatory effect of continuous release of lithium might be investigated further. From the results, it can also be speculated that when different concentrations of PGFs(Fe) and lithium in the GelMA structure are optimized, modulation of increasing GFAP levels is plausible for future studies.

GelMA-PGFs(Ti) has shown significantly increased IL-6 expression at 24 h (Figure 4) considering this lithium by itself may have helped to modulate this response with decreased values seen for GelMA+PGFs(Ti) ("+" represents lithium presence).

After 72 h of recovery incubation with fresh growth media, a second qPCR run was performed to assess the recovery from LPS-induced increased GFAP expression. The results suggested that GFAP levels were more moderate than the initial 24 h results with groups that included lithium, the fold change in GFAP expression for the GelMA-PGFs(Fe) group was shown to not have a statistically significant decrease compared to other experimental groups ($p = .07$) (Figure 5). Unfortunately, the expression level of IL-6 at 72 h was undetermined, as the Ct values were too high, and the raw data exported showed "undetermined." Therefore, IL-6 expression at 72 h was not presented in the results.

In order to visualize primary astrocytes cultured in 3D in GelMA, GelMA-PGF samples GFAP unconjugated mouse IgG (0.2 mg/mL),

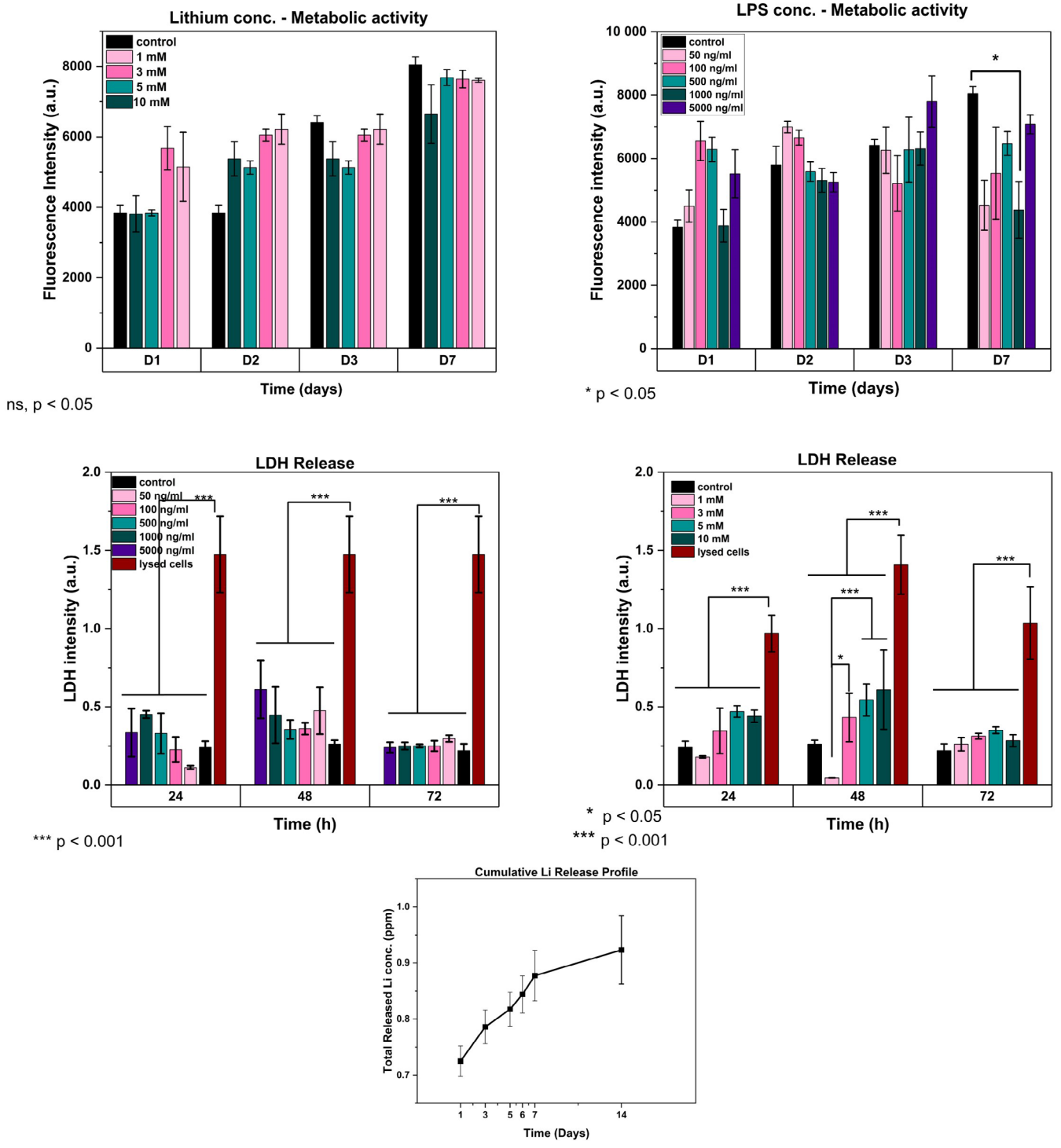

FIGURE 4 Alamar Blue-Metabolic activity results; five different concentrations of LPS treated via addition into growth media after cell-seeded into GelMA ($n = 3$, One Way ANOVA $p < .05$) LDH release to media over time from cells cultured into GelMA hydrogels and treated with LPS in growth media with increasing concentrations, positive control was GelMA only (no LPS), and negative control (lysed cells) was cells lysed 45 min prior to LDH assay ($n = 3$, One way ANOVA, $^{***}p < .001$) ICP-OES results cumulative profile of detected lithium release to water from GelMA hydrogels over time ($n = 5$, error bars: SD).

monoclonal primer antibodies have been utilized. Secondary antibody of Alexafluor-488 conjugated goat anti-mouse IgG, H&C has been used along with DAPI and PI counterstains. The resulting fluorescent images can be seen in Figure 6.

The first and second images of Figure 6 show that treatment with LPS has led to increased expression of GFAP, which is consistent with the results of qPCR. Among groups without lithium, GelMA-PGFs(Ti) showed the highest level of GFAP expression, while GelMA-

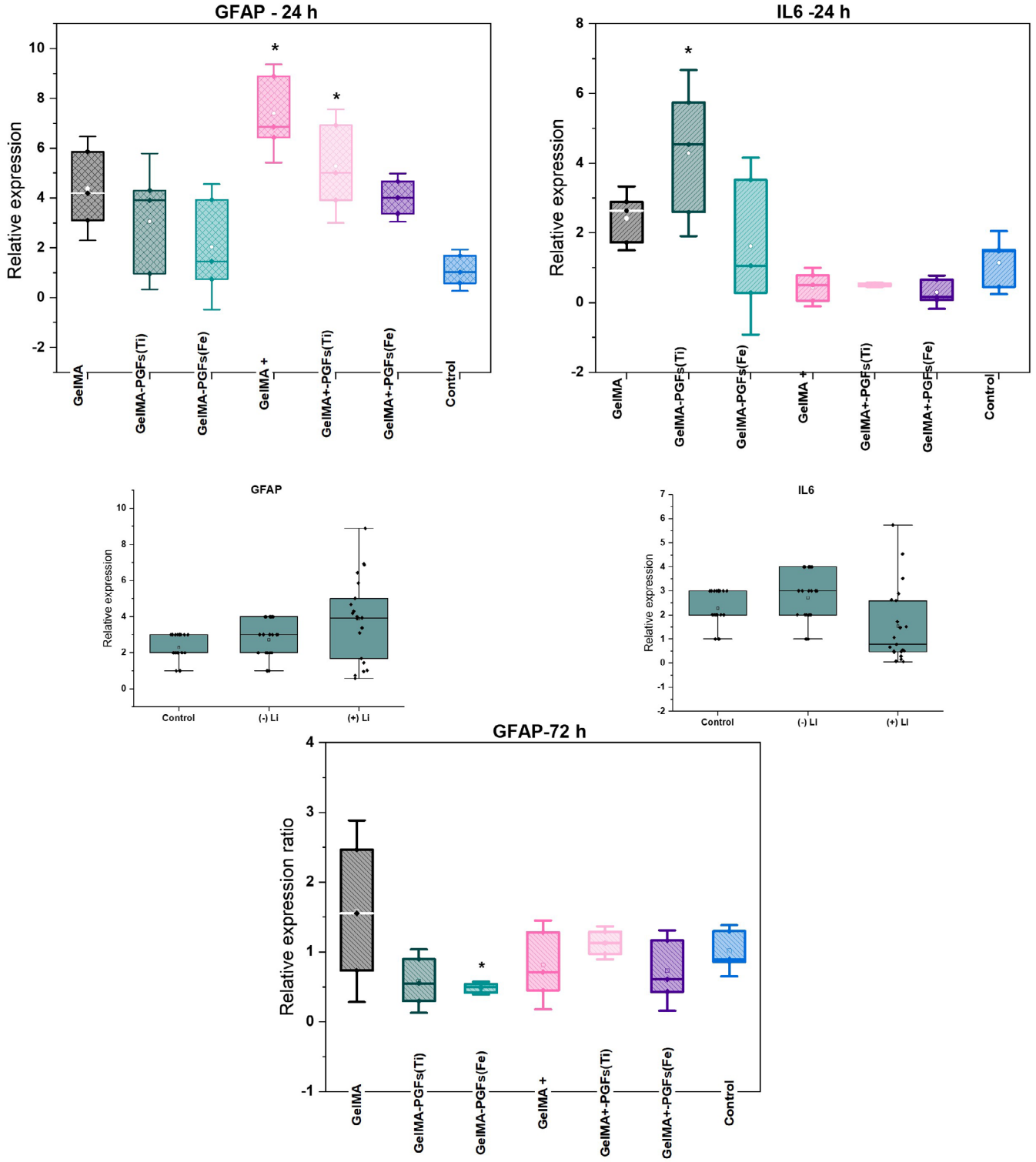

FIGURE 5 Relative expression of GFAP and IL-6 in 24 and 72 h for primary astrocytes cultured into GelMA, GelMA-PGFs, and GelMA/Li-PGFs hydrogels at 24 and 72 h under the stimulation of LPS. (Control: GelMA only no LPS stimulation, see in Table 1, $n = 3$, error bars: SD, OneWay ANOVA, ns, $p < .05$).

PGFs(Fe) showed the lowest. The presence of lithium in combination with PGFs, and possibly due to the release of (Fe) and (Ti) ions during the degradation of phosphate glass fibers, has resulted in a decrease in the expression of GFAP, as evidenced by reduced green fluorescence in GelMA/Li-PGFs(Fe) and GelMA/Li-PGFs(Ti) compared to those without lithium (Figure 6).

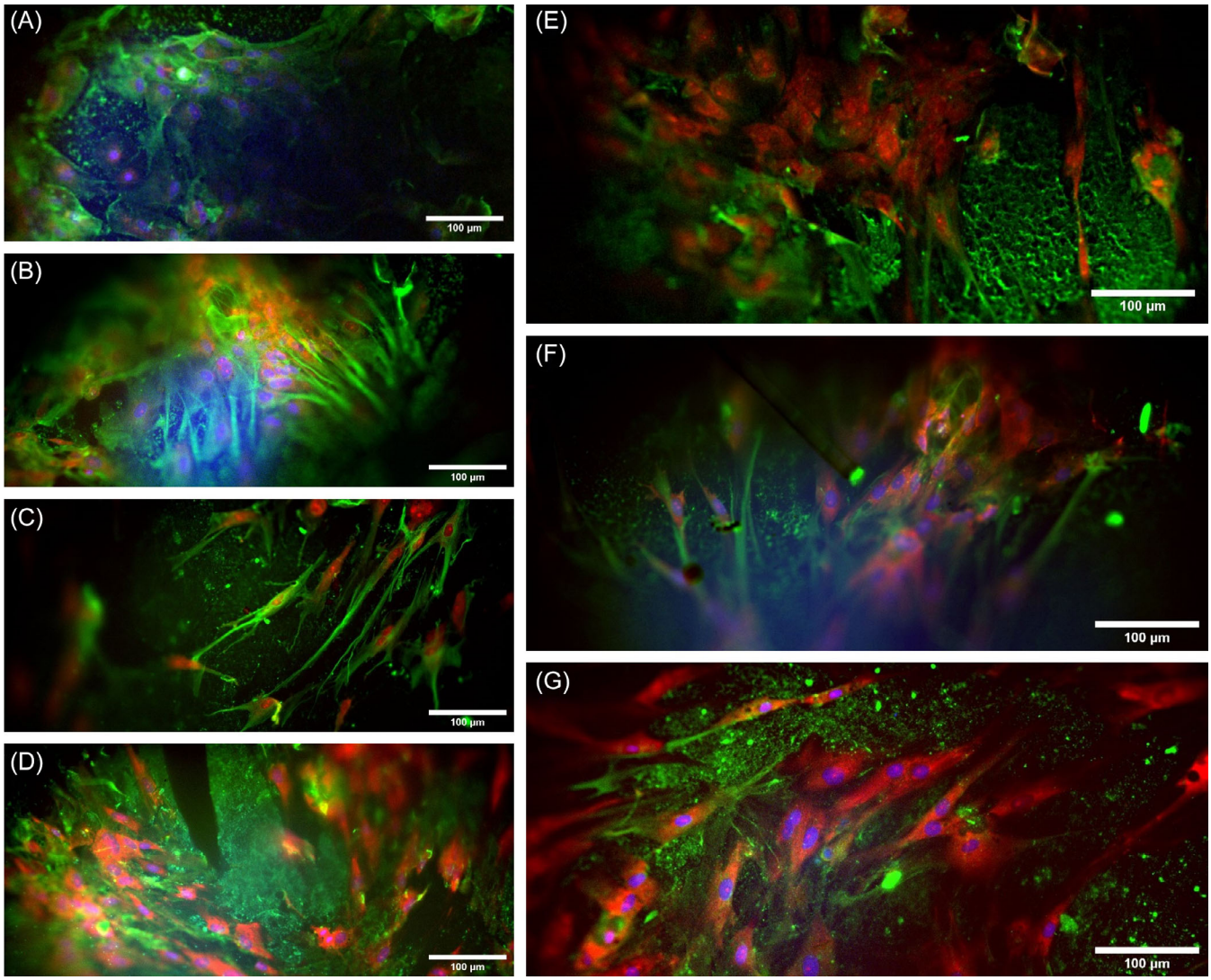

FIGURE 6 Immunofluorescence images were taken on confocal on 72 h of recovery after 24 h of LPS treatment (green: GFAP, blue: DAPI, red: PI) for the samples of a) GelMA only (no LPS), b) GelMA(+LPS), c) GelMA-PGFs(Fe) (+LPS), d) GelMA-PGFs(Ti) (+LPS), and lithium-loaded samples of e) GelMA only/Li (+LPS), f) GelMA-PGFs(Fe)/Li (+LPS) and g) GelMA-PGFs(Ti)/Li (+LPS). Scale bars:100 µm.

4 | DISCUSSION

SCIs have complex pathophysiology following primary injury, so promoting regeneration cannot be achieved through a single drug or recovery procedure. Rather, multiple approaches may be necessary for an achievable repair.[32] Engineered biomaterials for functional recovery in the CNS can play a vital role in treatment designs and developing tissue constructs that provide the capability to promote directionality within the neural site for aligned axonal regeneration as well as leading to manageable inflammatory response and modulated glial scarring is desired.

As previously shown by our previous work,[24] developed GelMA-PGF constructs that can provide directionality growth for glial cells. In the work presented here, the same constructs have been investigated for *in vivo* biocompatibility and show manageable immune responses in a rat subcutaneous implant model.

Though the *in vivo* results are limited in the presented work in terms of the ultimate target tissue that the construct is designed for, as shown with the subcutaneous rat model which has obviously environmental and vascular differences compared to the spinal cord milieu, it is believed that results give a broad understanding of feasibility of the materials and host response to the GelMA-PGFs constructs for future translational for CNS applications.

Titanium dioxide containing PGFs has shown intensified neural growth (red channel) in Figure 2 in this study that may merit further attention for future studies in neural tissue regeneration studies as previously reported[33] their work demonstrated titanium dioxide when used as a substrate for neural cells showed increased the neural growth. Additionally, recent research[34] revealed a significant improvement in neurite outgrowth when TiO_2 was employed in nanoparticle form with PC12 cells *in vitro*. The results from our study can be correlated with these existing findings offering insights for

potential future applications of titanium dioxide-containing bioactive materials.

Furthermore, in this work, to evaluate and improve bioactivity in terms of modulating inflammation and glial scar formation in SCIs the preliminary basis of introducing lithium to GelMA hydrogel constructs via lithium chloride loading has been explored by aiming to show its potential to mitigate inflammatory response and astrocyte reactivity on *in vitro* LPS stimulated primary astrocytes.

At high dosages, lithium can cause severe and debilitating side effects, but it can also function as a nutrient, transporting and absorbing vitamins B12 and folate, modulating neurotransmission, and acting on a variety of biochemical processes. There are numerous studies that show lithium can stimulate the proliferation of neural and stem cells.[35–37] There has been a substantial body of research to suggest that lithium therapy has the potential as a treatment for a variety of neurological disorders, including traumatic brain injury (TBI), Alzheimer's disease, Parkinson's disease, amyotrophic lateral sclerosis (ALS), chronic pain, mercury toxicity, depression/anxiety, alcoholism, and drug addiction.[38–40] In other respects, toxicity from lithium is likely to be observed when the serum concentrations reach above 1.5 mM and above values since the safe and therapeutic dosage interval of lithium levels have reported as 0.6–1.2 mM.[37] Thus, regarding the utilization of lithium, its release profile, method of application, and concentration to use as a compound for regenerative medicine applications should be well defined prior to use. Estrado et al. (2013) have reported lithium has shown significant amelioration in the disease pathology and rescued memory impairments in a mouse Alzheimer's model.[41] Li et al.[19] have reported that lithium exerts potent anti-inflammatory effects *in vivo* by reducing the expression of pro-inflammatory cytokines and chemokines.[19] Additionally, lithium stimulates T cells (Ohteki et al., 2000) and enhances the survival of neural stem cells.[42,43] Thus, lithium has many advantageous effects that make it potentially a good candidate for neuro-regeneration for spinal cord injury applications. When taken orally (0.6–1.2 mmol/L for 6 weeks) in patients with chronic SCIs, lithium has been found effective in dealing with neuropathic pain even though it has not shown any significant changes in functional outcome and neurological classifications.[44]

In addition, though it was not significant with the performed set of experiments, it has shown relatively decreased GFAP expression in primary astrocyte cultures *in vitro* with GelMA-PGFs(Fe) constructs. In the long term, when optimized thoroughly, lithium loading in the GelMA structure may help with axonal regeneration by modulating glial scar tissue formation.

Furthermore, Li et al.[20] have also worked on the effect of lithium on LPS-induced astrocyte reactivity specifically on the inhibition of Toll-Like Receptor 4 (TLR4) which is attributed to inflammatory responses, and they have found that application of 1 mM $LiCl_2$ to *in vitro* LPS stimulated astrocytes, have ameliorated TLR4 expression and downregulated IL-6 and TNF-a production.[20] The results from this work also support their results in terms of decreased gene expression levels of IL-6 with lithium-loaded hydrogels (Figure 4) which has shown a 2.5-fold change of relative expression. However mechanistic details have not been determined. Acaz-Fonseca et al. (2019) have also established a model of reactive astrogliosis by exposing primary cortical astrocytes to 500 ng/mL LPS for 24 h and found that this stimulation has also shown enhanced expression of two of the main pro-inflammatory factors released by reactive astrocytes which are cytokine IL-6 and chemokine IL-10.[45] On the contrary in this work due to the polymeric network structure of 3D hydrogels compared to direct exposure of LPS to monolayer cultures, 500 ng/mL LPS application for 24 h has not resulted in significantly increased reactivity with primary astrocytes so that higher concentration of LPS of 1 μg/mL were examined and resulted in higher stimulation and overexpression levels of GFAP.

Morphological and physiological changes in astrocytes are often described as 'astrogliosis' or 'reactivity of astrocytes', which are usually associated with an increase in the GFAP protein and cellular hypertrophy, which may or may not be associated with cell proliferation.[21,46,47] The confocal images obtained in this study have revealed morphological changes in primary astrocytes grown on GelMA/Li with LPS-positive samples, as demonstrated in Figure 5. Specifically, these cells exhibited an elongated morphology with cell bodies and tendrils (pointed with arrows in Figure 5). However, it is important to note that reactive astrogliosis can have both deleterious and beneficial effects, depending on the context.[7] Previous research by Seidlits et al. (2010)[48] showed that astrocytes grown on hydrogels expressed lower levels of GFAP compared to those grown on glass coverslips, which exhibit a reactive phenotype. This suggests that astrocytes cultured in a 3D environment may be in a more quiescent state.[48]

5 | CONCLUSION

This work contributes to neural tissue engineering applications, with the successful development and *in vitro* and *in vivo* characterization and performance of two different inorganic and organic biomaterial-based constructs. The presence of PGFs aligned in GelMA structure has significantly improved the directional growth with glial cells previously, besides increasing the total stiffness of the constructs in comparison with the very soft GelMA-only scaffolds. Following this, *in vivo* biocompatibility results have shown that GelMA-PGFs (Fe) construct shows better performance as well as an ability to modulate glial scarring over GFAP regulation and *in vivo* biocompatibility via histological analyses. The study also sought to assess the effect of lithium on reactive astrocytes presented via loading within GelMA-PGFs constructs. The safe dose of 1 mM lithium as determined from experiments was used and the results showed a relatively reduced fold change in the expression of IL-6 but were unable to prove the hypothesized amelioration in LPS-induced *in vitro* astrocyte reactivity over GFAP expression level. However, it can be speculated that when further investigations on presentation, concentration, and release of lithium are done this may help with axonal regeneration by reducing glial scar tissue formation. Moreover, it is also worth investigating for future studies that the feasibility of introducing lithium via glass fibers as in incorporating lithium directly into phosphate glass formulation which could provide delivery of lithium in a more controlled manner

and construct development will be simplified for further translational studies.

AUTHOR CONTRIBUTIONS

Zalike Keskin-Erdogan: Conceptualization, investigation, methodology, validation, visualization, writing (original draft preparation), funding acquisition. **Nandin Mandakhbayar, Gang Shi Jin, Yu-Meng Li:** investigation, methodology, writing (review & editing). **David Y. S. Chau, Richard M. Day:** supervision and writing (review & editing). **Hae-Won Kim, Jonathan C. Knowles:** resources, project administration, supervision, writing (Review & editing).

ACKNOWLEDGMENTS

The authors acknowledge the valuable contributions from the ZKE's completed PhD thesis, which is the foundation for this research work. The authors also would like to thank Dr. George Georgiou, Dr. Graham Palmer, Dr Nicola Mordan, and Dr Nazanin Owji for their help in the laboratory. The graphical abstract and figure 1 was created by authors using BioRender.com.

FUNDING INFORMATION

This research was funded by the Republic of Turkiye Ministry of National Education under the scholarship program of Selection & Placement of Students to be sent abroad for post-graduate studies (YLSY), which supported this work and PhD study of first author Zalike Keskin-Erdogan. The authors also acknowledge the funding support of the National Research Foundation of Korea (RS-2023-00220408 and MRC 2021R1A5A2022318).

CONFLICT OF INTEREST STATEMENT

The authors declare no conflicts of interest.

DATA AVAILABILITY STATEMENT

The data that support the findings of this study are available from the corresponding author upon reasonable request.

ORCID

Zalike Keskin-Erdogan https://orcid.org/0000-0001-6789-6954
David Y. S. Chau https://orcid.org/0000-0001-9200-6749
Jonathan C. Knowles https://orcid.org/0000-0003-3917-3446

REFERENCES

1. Cao J, Sun C, Zhao H, et al. The use of laminin modified linear ordered collagen scaffolds loaded with laminin-binding ciliary neurotrophic factor for sciatic nerve regeneration in rats. *Biomaterials*. 2011;32(16):3939-3948. doi:10.1016/J.BIOMATERIALS.2011.02.020
2. Li G, Xiao Q, Zhang L, Zhao Y, Yang Y. Nerve growth factor loaded heparin/chitosan scaffolds for accelerating peripheral nerve regeneration. *Carbohydr Polym*. 2017;171:39-49. doi:10.1016/J.CARBPOL.2017.05.006
3. Malinovskaya Y, Melnikov P, Baklaushev V, et al. Delivery of doxorubicin-loaded PLGA nanoparticles into U87 human glioblastoma cells. *Int J Pharm*. 2017;524(1–2):77-90. doi:10.1016/J.IJPHARM.2017.03.049
4. Meyer C, Stenberg L, Gonzalez-Perez F, et al. Chitosan-film enhanced chitosan nerve guides for long-distance regeneration of peripheral nerves. *Biomaterials*. 2016;76:33-51. doi:10.1016/J.BIOMATERIALS.2015.10.040
5. Chai Q, Jiao Y, Yu X. Hydrogels for biomedical applications: their characteristics and the mechanisms behind them. *Gels*. 2017;3:6. doi:10.3390/gels3010006
6. Xia Y, Yang R, Wang H, et al. Biomaterials delivery strategies to repair spinal cord injury by modulating macrophage phenotypes. *J Tissue Eng*. 2022;13:204173142211430. doi:10.1177/20417314221143059
7. Liddelow SA, Barres BA. Reactive astrocytes: production, function, and therapeutic potential. *Immunity*. 2017;46(6):957-967. doi:10.1016/j.immuni.2017.06.006
8. Bradbury EJ, Burnside ER. Moving beyond the glial scar for spinal cord repair. *Nat Commun*. 2019;1–15:3879. doi:10.1038/s41467-019-11707-7
9. Oberheim NA, Goldman SA, Nedergaard M. Heterogeneity of astrocytic form and function. *Methods Mol Biol*. 2012;814:23. doi:10.1007/978-1-61779-452-0_3
10. Alizadeh A, Dyck SM, Karimi-Abdolrezaee S. Traumatic spinal cord injury: an overview of pathophysiology, models and acute injury mechanisms. *Front Neurol*. 2019;10:282. doi:10.3389/FNEUR.2019.00282
11. Moeendarbary E, Weber IP, Sheridan GK, et al. The soft mechanical signature of glial scars in the central nervous system. *Nat Commun*. 2017;8:1-11. doi:10.1038/ncomms14787
12. Yang Z, Wang KKW. Glial fibrillary acidic protein: from intermediate filament assembly and gliosis to neurobiomarker. *Trends Neurosci*. 2015;38(6):364-374. doi:10.1016/J.TINS.2015.04.003
13. Tanaka T, Narazaki M, Kishimoto T. IL-6 in inflammation, immunity, and disease. *Cold Spring Harb Perspect Biol*. 2014;6:a016295.
14. Chin JS, Milbreta U, Becker DL, Chew SY. Targeting connexin 43 expression via scaffold mediated delivery of antisense oligodeoxynucleotide preserves neurons, enhances axonal extension, reduces astrocyte and microglial activation after spinal cord injury. *J Tissue Eng*. 2023;14:204173142211457. doi:10.1177/20417314221145789
15. Zhang L, Lei Z, Guo Z, et al. Reversing glial scar Back to neural tissue through NeuroD1-mediated astrocyte-to-neuron conversion. *BioRxiv*. 2018;261438. doi:10.1101/261438
16. Bradbury EJ, Moon LDF, Popat RJ, et al. Chondroitinase ABC promotes functional recovery after spinal cord injury. *Nature*. 2002;416(6881):636-640. doi:10.1038/416636a
17. Ceyzériat K, Ben Haim L, Denizot A, et al. Modulation of astrocyte reactivity improves functional deficits in mouse models of Alzheimer's disease. *Acta Neuropathol Commun*. 2018;6(1):104. doi:10.1186/s40478-018-0606-1
18. Silver J, Miller JH. Regeneration beyond the glial scar. *Nat Rev Neurosci*. 2004;5(2):146-156. doi:10.1038/nrn1326
19. Li H, Li Q, Du X, et al. Lithium-mediated long-term neuroprotection in neonatal rat hypoxia-ischemia is associated with antiinflammatory effects and enhanced proliferation and survival of neural stem/progenitor cells. *J Cereb Blood Flow Metab*. 2011;31(10):2106-2115. doi:10.1038/JCBFM.2011.75
20. Li N, Zhang X, Dong H, Zhang S, Sun J, Qian Y. Lithium ameliorates LPS-induced astrocytes activation partly via inhibition of toll-like receptor 4 expression. *Cellul Physiol Bichem*. 2016;38:714-725. doi:10.1159/000443028
21. Rivera AD, Butt AM. Astrocytes are direct cellular targets of lithium treatment: novel roles for lysyl oxidase and peroxisome-proliferator activated receptor-γ as astroglial targets of lithium. *Transl Psychiatry*. 2019;9(1):211. doi:10.1038/S41398-019-0542-2
22. Khan PK, Mahato A, Kundu B, et al. Influence of single and binary doping of strontium and lithium on in vivo biological properties of bioactive glass scaffolds. *Sci Rep*. 2016;6(September):1-18. doi:10.1038/srep32964
23. Jin Y, Xu L, Hu X, Liao S, Pathak JL, Liu J. Lithium chloride enhances bone regeneration and implant osseointegration in osteoporotic

conditions. *J Bone Miner Metab*. 2017;35(5):497-503. doi:10.1007/S00774-016-0783-6

24. Keskin-Erdogan Z, Patel KD, Chau DYS, Day RM, Kim HW, Knowles JC. Utilization of GelMA with phosphate glass fibers for glial cell alignment. *J Biomed Mater Res: Part A*. 2021;109(11):2212-2224. doi:10.1002/JBM.A.37206
25. Ahmed I, Collins CA, Lewis MP, Olsen I, Knowles JC. Processing, characterisation and biocompatibility of iron-phosphate glass fibres for tissue engineering. *Biomaterials*. 2004;25(16):3223-3232. doi:10.1016/j.biomaterials.2003.10.013
26. Joo NY, Knowles JC, Lee GS, et al. Effects of phosphate glass fiber-collagen scaffolds on functional recovery of completely transected rat spinal cords. *Acta Biomater*. 2012;8(5):1802-1812. doi:10.1016/j.actbio.2012.01.026
27. Noshadi I, Hong S, Sullivan KE, et al. In vitro and in vivo analysis of visible light Crosslinkable gelatin Methacryloyl (GelMA) hydrogels. *Biomater Sci*. 2017;5(10):2093-2105. doi:10.1039/C7BM00110J
28. Zhao D, Yu Z, Li Y, Wang Y, Li Q, Han D. GelMA combined with sustained release of HUVECs derived exosomes for promoting cutaneous wound healing and facilitating skin regeneration. *J Mol Histol*. 2020;51(3):251-263. doi:10.1007/S10735-020-09877-6
29. Lavrentev FV, Shilovskikh VV, Alabusheva VS, et al. Diffusion-limited processes in hydrogels with chosen applications from drug delivery to electronic components. *Molecules*. 2023;28(15):5931. doi:10.3390/molecules28155931
30. Forlenza OV, De-Paula VJR, Diniz BSO. Neuroprotective effects of lithium: implications for the treatment of Alzheimer's disease and related neurodegenerative disorders. *ACS Chem Neurosci*. 2014;5(6):443-450. doi:10.1021/cn5000309
31. Hashimoto R, Senatorov V, Kanai H, Leeds P, Chuang DM. Lithium stimulates progenitor proliferation in cultured brain neurons. *Neuroscience*. 2003;117(1):55-61. doi:10.1016/S0306-4522(02)00577-8
32. Ham TR, Leipzig ND. Biomaterial strategies for limiting the impact of secondary events following spinal cord injury. *Biomed Mater*. 2018;13(2):024105. doi:10.1088/1748-605X/aa9bbb
33. Carballo-Vila M, Moreno-Burriel B, Chinarro E, Jurado JR, Casañ-Pastor N, Collazos-Castro JE. Titanium oxide as substrate for neural cell growth. *J Biomed Mater Res: Part A*. 2009;90(1):94-105. doi:10.1002/JBM.A.32058
34. Koushali SK, Hamadanian M. Improvement of neurite outgrowth in PC12 cells by TiO_2, Au/TiO_2 and Ag/TiO_2 nanoparticles. *J Nanostruct*. 2023;13(2):325-340. doi:10.22052/JNS.2023.02.002
35. Cervantes P, Ghadirian AM, Vida S. Vitamin B12 and folate levels and lithium administration in patients with affective disorders. *Biol Psychiatry*. 1999;45(2):214-221. doi:10.1016/S0006-3223(97)00544-1
36. Ferensztajn-Rochowiak E, Rybakowski JK. The effect of lithium on hematopoietic, mesenchymal and neural stem cells. *Pharmacol Rep*. 2016;68(2):224-230. doi:10.1016/J.PHAREP.2015.09.005
37. Hedya SA, Avula A, Swoboda HD. Lithium toxicity. *Emerg Med Clin North Am*. 2021;12(2):511-531. doi:10.22374/cjgim.v8i2.73
38. Albayrak A, Halici Z, Polat B, et al. Protective effects of lithium: a new look at an old drug with potential antioxidative and anti-inflammatory effects in an animal model of sepsis. *Int Immunopharmacol*. 2013;16(1):35-40. doi:10.1016/J.INTIMP.2013.03.018
39. De-Paula VJ, Gattaz WF, Forlenza OV. Long-term lithium treatment increases intracellular and extracellular brain-derived neurotrophic factor (BDNF) in cortical and hippocampal neurons at subtherapeutic concentrations. *Bipolar Disord*. 2016;18(8):692-695. doi:10.1111/BDI.12449
40. Nassar A, Azab AN. Effects of lithium on inflammation. *ACS Chem Neurosci*. 2014;5(6):451-458. doi:10.1021/CN500038F
41. Trujillo-Estrada L, Jimenez S, De Castro V, et al. In vivo modification of Abeta plaque toxicity as a novel neuroprotective lithium-mediated therapy for Alzheimer's disease pathology. 2013;1. doi:10.1186/2051-5960-1-73
42. Willing AE, Zigova T, Milliken M, et al. Lithium exposure enhances survival of NT2N cells (hNT neurons) in the hemiparkinsonian rat. *Eur J Neurosci*. 2002;16(12):2271-2278. doi:10.1046/J.1460-9568.2002.02300.X
43. Ohteki T, Parsons M, Zakarian A, et al. Negative regulation of T cell proliferation and interleukin 2 production by the serine threoninekinase GSK-3. *J Exp Med*. 2000;192(1):99-104. doi:10.1084/jem.192.1.99
44. Yang ML, Li JJ, So KF, et al. Efficacy and safety of lithium carbonate treatment of chronic spinal cord injuries: a double-blind, randomized, placebo-controlled clinical trial. *Spinal Cord*. 2012;50:141-146. doi:10.1038/sc.2011.126
45. Acaz-Fonseca E, Ortiz-rodriguez A, Azcoitia I, Garcia-segura LM, Arevalo M. Notch signaling in astrocytes mediates their morphological response to an inflammatory challenge. *Cell Death Dis*. 2019;5:85. doi:10.1038/s41420-019-0166-6
46. Escartin C, Galea E, Lakatos A, et al. Reactive astrocyte nomenclature, definitions, and future directions. *Nat Neurosci*. 2021;24(3):312-325. doi:10.1038/s41593-020-00783-4
47. Pekny M, Pekna M, Messing A, et al. Astrocytes: a central element in neurological diseases. *Acta Neuropathol*. 2016;131(3):323-345. doi:10.1007/S00401-015-1513-1
48. Seidlits SK, Khaing ZZ, Petersen RR, et al. The effects of hyaluronic acid hydrogels with tunable mechanical properties on neural progenitor cell differentiation. *Biomaterials*. 2010;31(14):3930-3940. doi:10.1016/J.BIOMATERIALS.2010.01.125

SUPPORTING INFORMATION

Additional supporting information can be found online in the Supporting Information section at the end of this article.

How to cite this article: Keskin-Erdogan Z, Mandakhbayar N, Jin GS, et al. Lithium-loaded GelMA-Phosphate glass fibre constructs: Implications for astrocyte response. *J Biomed Mater Res*. 2024;1-13. doi:10.1002/jbm.a.37686